Quantitative proteomics of the Cav2 channel nano-environments in the mammalian brain

Catrin Swantje Müller[a], Alexander Haupt[a,c], Wolfgang Bildl[a], Jens Schindler[a], Hans-Günther Knaus[d], Marcel Meissner[e], Burkhard Rammner[f], Jörg Striessnig[g], Veit Flockerzi[e], Bernd Fakler[a,b,1], and Uwe Schulte[a,c,1]

[a]Institute of Physiology II, University of Freiburg, 79108 Freiburg, Germany; [b]Center for Biological Signaling Studies, 79104 Freiburg, Germany; [c]Logopharm GmbH, 79108 Freiburg, Germany; [d]Division of Molecular and Cellular Pharmacology, Medical University Innsbruck, A-6020 Innsbruck, Austria; [e]Experimentelle und Klinische Pharmakologie und Toxikologie, Universität des Saarlandes, 66421 Homburg, Germany; [f]Scimotion, 22761 Hamburg, Germany; and [g]Department of Pharmacology and Toxicology, Center of Molecular Biosciences, University of Innsbruck, A-6020 Innsbruck, Austria

This Feature Article is part of a series identified by the Editorial Board as reporting findings of exceptional significance.

Local Ca^{2+} signaling occurring within nanometers of voltage-gated Ca^{2+} (Cav) channels is crucial for CNS function, yet the molecular composition of Cav channel nano-environments is largely unresolved. Here, we used a proteomic strategy combining knockout-controlled multiepitope affinity purifications with high-resolution quantitative MS for comprehensive analysis of the molecular nano-environments of the Cav2 channel family in the whole rodent brain. The analysis shows that Cav2 channels, composed of pore-forming α1 and auxiliary β subunits, are embedded into protein networks that may be assembled from a pool of ∼200 proteins with distinct abundance, stability of assembly, and preference for the three Cav2 subtypes. The majority of these proteins have not previously been linked to Cav channels; about two-thirds are dedicated to the control of intracellular Ca^{2+} concentration, including G protein-coupled receptor-mediated signaling, to activity-dependent cytoskeleton remodeling or Ca^{2+}-dependent effector systems that comprise a high portion of the priming and release machinery of synaptic vesicles. The identified protein networks reflect the cellular processes that can be initiated by Cav2 channel activity and define the molecular framework for organization and operation of local Ca^{2+} signaling by Cav2 channels in the brain.

calcium channel | Ca^{2+} signaling | proteome | biochemistry | mass spectrometry

In CNS neurons, voltage-activated calcium (Cav) channels initiate a multitude of signaling processes by delivering calcium ions (Ca^{2+}) to the cytoplasm that serve as second messengers (1, 2). Despite this rather unselective trigger mechanism, Ca^{2+}-dependent signaling is endowed with high specificity and reliability by tightly restricting the Ca^{2+} signal, a transient increase in the intracellular Ca^{2+} concentration ($[Ca^{2+}]_i$) to very local spatiotemporal domains by means of a variety of Ca^{2+} buffer systems (3, 4). Within such local domains, $[Ca^{2+}]_i$ drops from hundreds of micromolar at the inner vestibule of the channel to values below 10 μM at a distance of several tens of nanometers from the Cav channel (3–5). Consequently, most Ca^{2+}-dependent signaling systems necessarily reside within these spatial boundaries (5–7) that may be termed nano-environments.

Nano-environments are of particular relevance for a number of processes in the dendritic and synaptic compartments, including neurotransmitter release, regulation of excitability, excitation–transcription coupling, synaptic plasticity, or axonal growth (5, 8–11). Many of these and a number of further processes are triggered by the subfamily 2 of Cav channels comprising the three members Cav2.1, 2.2, and 2.3 that conduct P/Q-type, N-type, and R-type Ca^{2+} currents, respectively (12). These channels are thought to be assembled from pore-forming α1 subunits and two distinct types of auxiliary subunits, Cavβ1-β4 and α2δ1-δ4; Cavγ2-γ8 have also been suggested as accessory subunits (13–15). Although the channel core complex has been extensively studied, the nano-environments of Cav2 channels have escaped direct

investigation, mostly because of technical limitations precluding their comprehensive proteomic analysis. Such unbiased analysis, however, is ultimately required for molecular understanding of the Cav2-mediated signaling.

Proteomic analysis of membrane-associated signaling networks represents a major technical challenge, particularly when native (not genetically manipulated) tissue is used as source material. Antibody-based affinity purification (AP) combined with quantitative MS is a target-directed approach, which, theoretically, allows for strong enrichment of both target proteins and more stably associated partners with tight control of specificity and interaction stringency (16). In fact, AP-based proteomics were successfully used for identification of accessory subunits and regulators of various ion-channel proteins (17–23). Notwithstanding, there remain several sources of error that are aggravated considerably when approaching protein networks such as those comprising nano-environments. First, solubilization conditions, generally a compromise between efficiency and preservation of protein–protein interactions, must be carefully adjusted. Second, specificity and selection biases of antibodies (ABs) must be well-controlled, because protein networks offer an increased surface for nonspecific binding and may obscure access of ABs to their epitopes. Finally, reliable identification of less-abundant or smaller proteins requires high-resolution quantitative MS (24). In the light of these concerns, previous efforts to identify proteins associated with Cav channels (25, 26) might have missed important components or contained false-positive interactors.

Here, we use a proteomic approach that combines a multipronged AP using optimized solubilization conditions, multiple ABs to distinct epitopes, and source material from wild-type (WT) and knockout animals together with high-resolution quantitative nanoflow tandem MS (nano–LC-MS/MS) and a tiered data-analysis procedure to identify proteins reconstituting the nano-environments of Cav2 channels in the mammalian brain. The identified Cav2 channel proteome provides a comprehensive set of data that serves as a roadmap for ultra-structural and functional analyses of local Ca^{2+} signaling by these key channels of synaptic transmission and plasticity.

Results

Isolation and Analysis of Cav2 Channel Nano-Environments. The experimental approach used to determine the nano-environments of Cav2 channels is illustrated in Fig. 1A.

Plasma membrane-enriched protein fractions were prepared from total brain of adult rats, WT mice, and mice with targeted deletions of either Cav2 α1 or Cav β subunits [Cav2.1 (27), Cav2.2 (28), Cav2.3 (29), Cavβ2 (30), Cavβ3 (31), and Cavβ4 (32)]. To optimize solubilization conditions that retained intact nano-environments, membrane fractions were solubilized with a set of detergent buffers of variable stringency (*Material and Methods*) and centrifuged under conditions leaving micelles with an estimated size (diameter) of up to ∼70 nm in the supernatant (Fig. S1). The yield of solubilized Cav2 α1 protein displayed a wide range as visualized by Western-probed gel separations. Thus, digitonin (33) solubilized only small amounts of the Cav2 α1 protein in the membrane fractions, whereas buffers CL-91 and CL-114 solubilized ∼50% and ∼95% of the Cav2 α1 protein, respectively (Fig. 1B *Left*). All solubilization conditions were compatible with subsequent APs; the amounts of Cav2 α1 retained by the affinity matrix in CL-91 and CL-114, however, exceeded that obtained with digitonin by about 10-fold (Fig. 1B *Right*). Because of its efficient yield of Cav2 α1 protein and its intermediate stringency (22, 34), the solubilization buffer CL-91 was used for most of the APs of Cav2 nano-environments.

For these APs, a set of 14 different ABs was applied, each directed against distinct epitopes either in the α1 subunits of the three Cav2 channel subtypes or the four different Cav β subunits (Fig. 1A, arrows) (*Material and Methods*); an additional AB targeted the Cav γ2 and γ3 proteins (*anti-γ2/3*) (22). This multiepitope strategy was used to eliminate the errors frequently introduced into APs of protein complexes by individual ABs because of their specific binding properties. Thus, ABs are often selective for complexes of particular subunit compositions over others, and/or they interfere with the integrity of complexes by high-affinity interaction with their target epitope (35). Off-target effects inherent to ABs through direct binding of proteins different from their target (cross-reactivity) were circumvented by the parallel use of Cav2 subunit knockout animals.

Complete eluates of all APs obtained with the different ABs from solubilized membrane fractions of WT and knockout animals were analyzed by high-resolution nano–LC-MS/MS on a hybrid linear ion trap/Fourier transform mass spectrometer (LTQ-FT Ultra). This provided data on both the identity (through fragmentation MS/MS spectra recorded by the ion trap) and the amount (through MS spectra over time measured in the ICR cell) of proteins in each of the eluates. The amount of each protein was quantified from the peak volumes (PVs; integral of MS signal intensity in the *m/z*-retention time plane) (22, 36) (Fig. 1A) of multiple tryptic peptides. Values determined for PVs with standard protein mixtures (ranging from 0.1 to 1,000 femtomoles) showed that the dynamic range of this label-free quantification extends over three to four orders of magnitude.

Quantitative data on protein amounts together with the subtype-specificity profile of the *anti-Cav* ABs (Fig. S2) and a three-staged filter were subsequently used to extract high-confidence protein constituents of Cav2 nano-environments from the multiple APs with the *anti-Cav* ABs (Fig. 1A). First, an abundance filter (Filter A) excluded all proteins identified in MS analyses by less
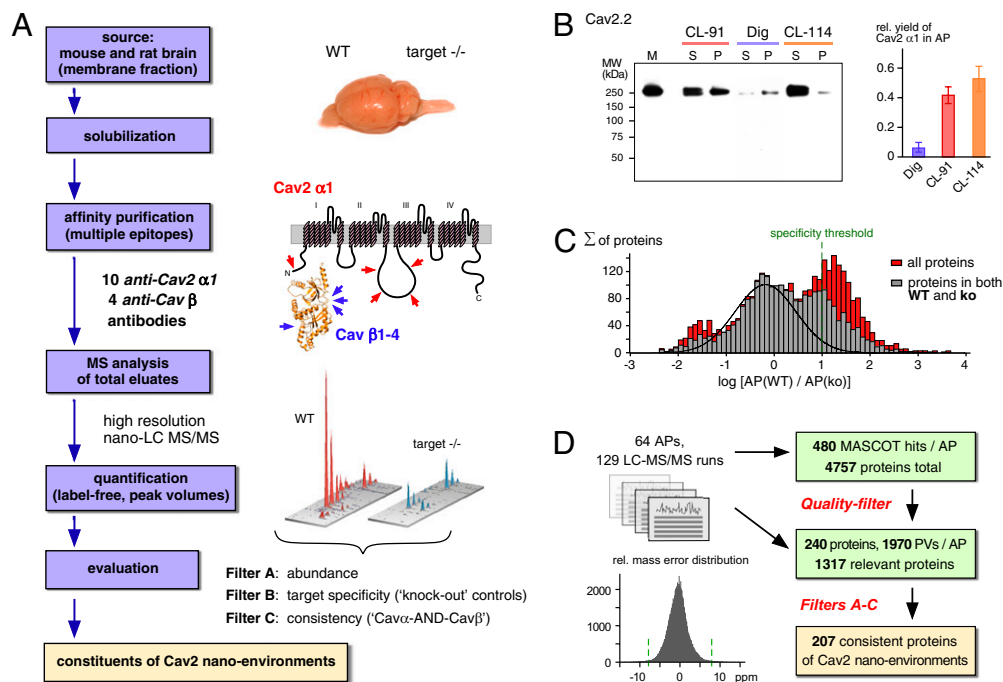

Fig. 1. Proteomic approach used for analysis of Cav2 nano-environments in the mammalian brain. (A) Workflow of the proteomic analysis as detailed in the main text. (B) Solubilization efficiency of Cav2.2 channels under various conditions (input) and retrieval of Cav2 α1 proteins in subsequent APs (output). (*Left*) Solubilized (S) and nonsolubilized (P) protein fractions obtained with buffers CL-91, CL-114, and digitonin (Dig) from rat brain membranes (M), resolved by SDS/PAGE and Western-probed with the *anti–Cav2.2-c* antibody. (*Right*) Relative yield of the Cav2 α1 proteins (mean ± SD) determined by quantitative MS analysis in five APs using the indicated solubilization buffers and all *anti-Cav2* α1 antibodies. (C) Determination of target specificity by abundance thresholds. Histogram plot summarizing abundance ratios (binned in logarithmic intervals; division of protein amounts obtained with Cav2 subunit-specific ABs in APs from WT and the respective knockout brains) of all proteins in all APs. Stacked bars in red are proteins exclusively detected in APs from WT or knockout brains. Continuous line represents distribution of the nonspecific proteins as obtained from fitting the sum of two Gaussians to the data; high-confidence threshold for specificity is indicated by the dashed line in green. (D) Summary of MS analyses used for identification of the protein constituents of Cav2 nano-environments. (*Inset*) Distribution of precursor mass error in ppm of all peptides identified by database searches with Mascot; green lines indicate *m/z* tolerance (± 8 ppm) used for PV assignment.

than two different peptides or that exhibited total PVs of less than ten times the detection threshold of the mass spectrometer. For Filter B, the remaining proteins were evaluated for their target-specific copurification with the *anti-Cav* ABs using membrane fractions from Cav subunit knockout mice and preimmunization IgGs as negative controls. Target specificity was defined by threshold values established in abundance-ratio histograms, which, for each protein, compared its amount in APs with *anti-Cav* ABs from WT and the respective target (Cav subunit) knockout mice (Fig. 1C) and/or its amount in APs (from rat brain) with *anti-Cav* ABs and a pool of preimmunization IgGs. Accordingly, all proteins enriched by more than 25-fold in APs with *anti-Cav* ABs versus control IgGs (positive filter) and not dubbed unspecific by the knockout control (amount in APs from WT less than 10 times the amount from the respective target knockout; negative filter) (Fig. 1C) were selected. Finally, Filter C analyzed the extracted candidate proteins for their consistency across the Cav2 α1 and Cav β APs. Acceptance of any protein required its appearance in (*i*) the majority of APs with at least one of three sets of α1-directed ABs and in (*ii*) APs with at least one of the Cav β-targeting ABs (Cavα-AND-Cavβ criterion); passing this criterion, thus, implied specific copurification with at least three different *anti-Cav* ABs. Accordingly, Filter C eliminated candidates with either lower abundance in the brain or less stable interaction with Cav2 channel-associated networks and enriched for candidates that robustly integrate into Cav2 nano-environments.

In summary, 64 APs were analyzed in 129 nano–LC-MS/MS runs that identified an average of 240 proteins per AP (with an average of 1,970 PVs assigned per AP) (Fig. 1D). After the three-stage filtering outlined above, 207 proteins were annotated as final constituents of the Cav2 nano-environments in the whole rat brain.

Core of Cav2 Channels. The proteins most effectively purified over the complete set of *anti-Cav* ABs were the α1 subunits, Cav2.1–Cav2.3, and the four Cav β subunits, Cavβ1–Cavβ4. MS retrieved large numbers of peptides for each of these Cav proteins (98, 93, and 80 different peptides for Cav2.1–Cav2.3; 25, 25, 22, and 31 peptides for Cavβ1–Cavβ4, respectively), providing extensive coverage of their accessible primary sequences (Fig. 2A and Fig. S3).

Detailed analysis of the protein amounts obtained with a subset of *anti-Cav* ABs using PVs normalized to the number of MS-accessible amino acids (abundance$_{norm}$; *SI Materials and Methods*) showed that Cav2 α1 and Cav β subunits were purified in about equimolar ratios and that this robust copurification was independent of the AB and buffer system used for solubilization (Fig. 2B). In contrast, the α2δ proteins α2δ1–3 were identified (by MS/MS spectra) only in APs using digitonin for solubilization, where their molar abundance was less than 10% of that obtained for the Cav2 α1 and Cav β subunits (Fig. 2B). In APs with the CL buffers, evaluation of PVs corresponding to peptide signals identified in digitonin APs revealed molar ratios for α2δ to Cav2 α1 or Cav β proteins of 0.1–1% (Fig. 2B). The supposed Cav γ subunits, γ2–γ8, were not detected in any of the APs performed (Fig. 2B). Accordingly, the *anti-γ2/3* AB, targeting the most abundant Cav γ isoforms in the rat brain, failed to copurify any Cav2 α1 or Cav β subunits, but rather purified with high-efficiency AMPA-type glutamate receptor complexes (22). These results indicate that the core of Cav2 channels in the rodent brain is composed of a pore-forming α1 and an auxiliary β subunit (Fig. 3). Within this framework, heterogeneity is generated by distinct assembly profiles between these subunits and/or by splice variations (Fig. S3). Thus, relative quantification of the Cav β proteins in all α1-directed APs showed that Cav2.1–Cav2.3 are distinctly assembled with Cavβ1–Cavβ3, whereas Cavβ4 is the most abundant auxiliary subunit of all Cav2 channel subtypes (Fig. 2C), in good agreement with a previous report using radio-labeled toxins (37).
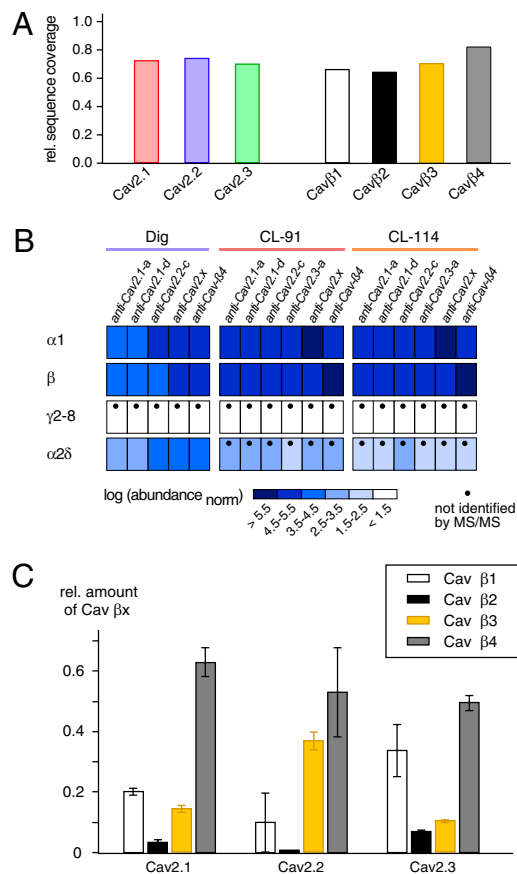
Fig. 2. Subunit composition of the Cav2 channel core. (*A*) Relative sequence coverage of the indicated Cav2 α1 and Cav β subunits by peptides retrieved in MS. (*B*) Abundance$_{norm}$ of the indicated proteins (color coded at logarithmic scale) in APs with the indicated solubilization buffers and *anti-Cav2* ABs. Note robust and stoichiometric association of Cav β and Cav2 α1 proteins under all conditions; α2δ copurified only in APs with digitonin as a solubilizing detergent, and γ2–8 failed to copurify with Cav2 channels. (*C*) Cav2 channel subtypes exhibit distinct profiles for assembly with the Cav β subunits as derived from quantification of Cavβ1–Cavβ4 proteins (mean ± SD, determined from relative amounts of Cav β) in APs with the *anti-Cav2* α1 ABs.

Proteome of Cav2 Channel Nano-Environments. In addition to the channel core, our proteomic analysis identified another 200 proteins as constituents of the Cav2 channel nano-environments in the whole rat brain (Fig. 3 and Table 1). All these partner proteins were specifically and consistently copurified with the Cav2 channels (passing Filters A–C) (Fig. 1A), although at different abundance (relative abundance in Table 1) and with distinct profiles for association with the Cav2 channel subtypes Cav2.1–Cav.2.3 (subtype preference in Table 1). The abundance$_{norm}$ values determined for the copurified proteins (over APs with all 14 *anti-Cav* ABs) ranged over more than three orders of magnitude, putting them into four categories related to the average amount of the Cav2 α1 proteins (used as reference). Thus, 40 proteins were copurified at amounts within one-half an order of magnitude of the reference (20%; marked = in rel. abundance in Table 1), 157 exhibited abundance$_{norm}$ values more than 3-fold beyond that of Cav2 α1 [designated < (109 proteins; 54.5%) or << (48 proteins; 24%) in Table 1], and only three extensively polymerizing tubulins (1.5%) exceeded the amount of Cav2 α1 by more than 3.3-fold (designated > in Table 1). An additional set of proteins copurified at similarly ranged abundance$_{norm}$ values but failing the consistency criterion (Filter C) were excluded from the
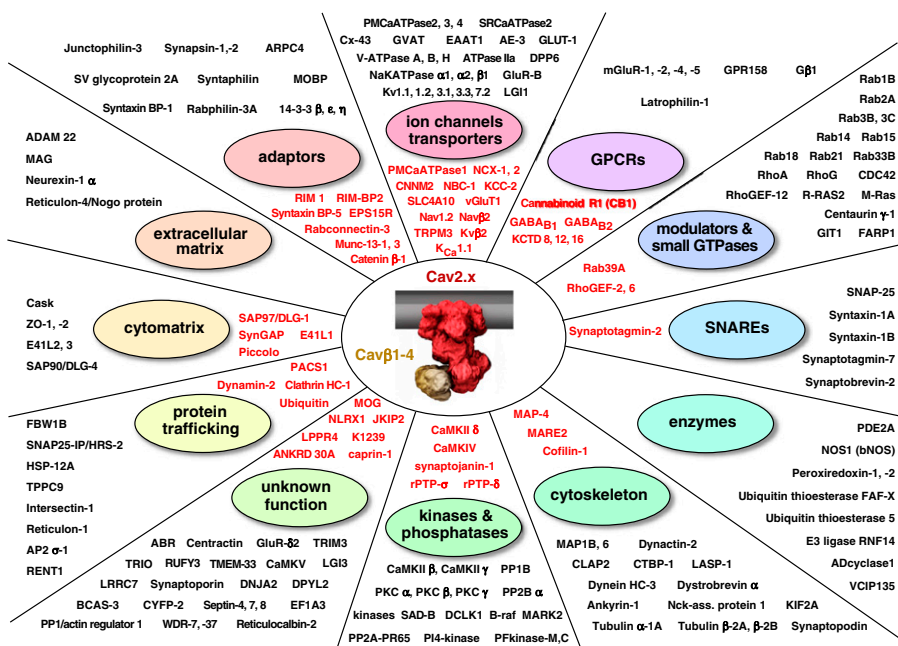
Fig. 3. Composition of the Cav2 channel nano-environments in the brain. Proteins identified by the proteomic approach with CL-91 solubilized membrane fractions categorized according to their primary biochemical function. Red font marks proteins copurified also under high-stringency conditions (CL-114). The Cav2 channel core made up from one α1 (Cav2.x) and one β subunit (Cavβ1–4) is depicted as a structural model in space-filling mode (generated with the Maya platform; *Materials and Methods* and Table S3).

final annotation of the Cav2 nano-environments (Table 1) and listed separately (Table S1).

Investigation of the subtype preference showed that the nano-environments of the three types of Cav2 channels are assembled from different pools of proteins (Fig. 4A): (*i*) those uniquely identified with either Cav2.1, Cav2.2, or Cav2.3 (68 of 204 proteins), (*ii*) those retrieved with at least two different types of Cav2 channels (84 proteins), and (*iii*) those common to all Cav2 channel subtypes (52 proteins). Accordingly, two-thirds of the nano-environment constituents are shared among Cav2.1–Cav2.3, whereas one-third is uniquely found with individual subtypes. The largest overlap was observed between Cav2.1 and Cav2.2 (99 of a total of 134 and 161 proteins, respectively) (Fig. 4A), in line with the shared role of both channels in presynaptic transmitter release (38).

Classification according to subcellular localization and topology as indicated in public databases (SwissProt, PubMed, and EMBL database) showed that more than one-half of the identified pro-
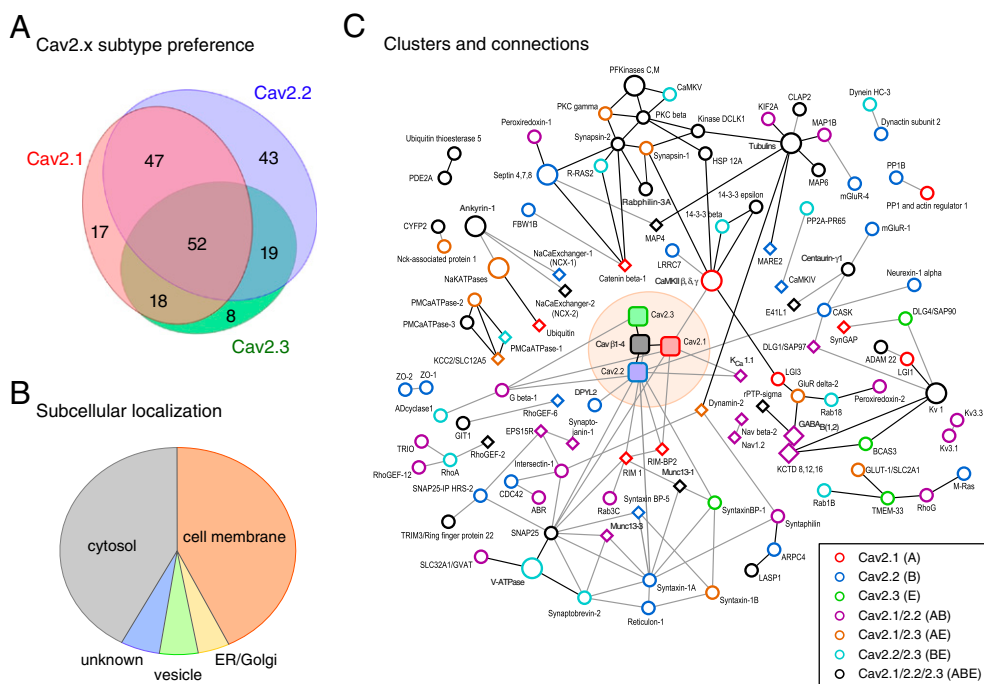
Fig. 4. Structural aspects of Cav2 nano-environments. (*A*) Overlap in subtype preference and (*B*) cellular localization of all proteins identified in the Cav2 proteome. (*C*) Structural connections and subclusters within Cav2 nano-environments as revealed by scientific literature and correlation analyses; shown are only protein constituents for which at least one direct protein–protein interaction was identified. Diamonds denote high-stringency interactors (Fig. 3), and color coding depicts subtype preference as indicated on the right; oversized symbols reflect grouping of several subunits. Lines represent direct protein–protein interactions as suggested in literature (gray) or identified by correlation analysis (black).

tein constituents of the Cav2 nano-environments are resident at membranes (Fig. 4B), most of them at the plasma membrane (89 of 207 proteins) (Table S2) and some at the ER/Golgi compartments (9) or in intracellular and synaptic vesicles (11). Many of these proteins are, in fact, membrane proteins (85 of 207), either integral to the membrane (78%) or membrane-associated through lipid anchors (22%). The remaining constituents of the Cav2 nano-environments are annotated as nonmembrane proteins mostly localized to the cytoplasm (87 of 207 proteins) (Fig. 4B), or they lack annotation of subcellular localizations (11 of 207 proteins). Proteins from other compartments, including nucleus, mitochondria, or lysosomes, that are frequently observed in proteomic work (16, 24) did not come through the three-tiered filtering as partners in Cav2-associated protein networks.

Analysis of their primary (biochemical) function showed that the proteins in the Cav2 nano-environments may be subdivided into 12 different categories with distinct numerical representation (Fig. 3): ion channels and transporters (44 of 207 proteins; 21.3%), G protein-coupled receptors (GPCRs, 13; 6.3%), modulators or small GTPases (21; 10.1%), members of the SNARE family of proteins (6; 2.9%), proteins with enzymatic activity (9; 4.3%), kinases and phosphatases (20; 9.7%), mediators of protein trafficking (12; 5.8%), proteins participating in the cytoskeleton (18; 8.7%), proteins of the cytomatrix (10; 4.8%), proteins contributing to extracellular matrix/cell adhesion (4; 1.9%), adaptor proteins (20; 9.7%), and proteins without annotated function(s) (30; 14.5%). Of this broad spectrum, several have been implicated in Ca^{2+}-dependent processes, predominantly in the synaptic compartment (8, 39), such as Ca^{2+}-triggered ion flux and enzymatic activities or the processing and fusion of synaptic vesicles; however, the vast majority of these proteins has not been linked to the nano-environments of Cav2 channels. Vice versa, proteins for which direct protein–protein interactions with Cav2 channels have been reported, including the SNARE proteins syntaxin-1 and SNAP-25 (40), CASK (41), DPYL2 (CRMP-2) (42), CaMKII (43), BK_{Ca} channels ($K_{Ca}1.1$) (17), and RIM1 (44), were all found effectively coassembled into the Cav2 nano-environments (Fig. 3, Table 1, and Table S4). In addition, the preferred GPCR-mediated depression of N-type Cav channels (over P/Q type) seen in functional studies (38) is reflected by the respective subtype preference found for the GPCRs in Cav2 nano-environments (Table 1). Interestingly, this preferred association with Cav2.2 was not only preserved through the integral GPCR subunits but also found for the recently identified auxiliary subunits of $GABA_B$ receptors, the potassium-channel tetramerization domain-containing (KCTD) proteins 8, 12, and 16 (34) (Table 1).

Stability and Connections of Cav2 Channel Nano-Environments. For protein networks, it is intrinsically difficult to determine which constituents are connected directly or indirectly and how stable are individual protein–protein interactions. Two further approaches were, therefore, used to gain insight into the formation of Cav2 nano-environments: APs under solubilization conditions of largely increased stringency and correlation analyses of all identified nano-environment constituents over all APs.

For APs under high-stringency conditions, a subset of six anti-Cav ABs (the same as in Fig. 2B) was used with the solubilization buffer CL-114, which, compared with CL-91, contained an increased concentration of an anionic detergent at a higher ionic strength (4-fold increase). Respective abundance ratios for CL-114 vs. CL-91 revealed values >0.25 for 60 proteins (Fig. 3, red and Table 1, bold), whereas for 147 proteins, CL-114 reduced protein abundance by more than 4-fold (Fig. 3, black and Table 1, regular). Thus, ~30% of the annotated proteins remained tightly associated with the Cav2 channel core, even when significant portions of the network, including most of the cytoskeleton and the tubulins, were removed (Fig. 3).

Correlation analysis of protein abundances across the 20 different anti-Cav APs performed on rat brain membranes (Materials and Methods) (Fig. S4A) revealed numerous connections between individual constituents of the Cav2 nano-environments and identified a series of subclusters forming within the network (Fig. 4C and Fig. S4B). Together with protein-interaction data from literature (mostly based on one-to-one interactions of proteins or protein domains), these connections provide a roadmap for the assembly of Cav2 nano-environments (Fig. 4).

Functions and Dynamics of the Cav2 Nano-Environments. Finally, the identified protein constituents (Fig. 3 and Table 1) were used together with data on their structure, function, and roles in cell physiology, as assessed from public databases and scientific literature, to derive a general concept for the operation and signaling by Cav2 nano-environments in the brain (Fig. 5).

Accordingly, the protein constituents of the Cav2 nano-environments may be subdivided into six functional groups (Fig. 5 Left) that closely cooperate to integrate the local Ca^{2+} signal and determine the output of a nano-environment. First, activation of the Cav2 channels leads to an initial increase in $[Ca^{2+}]_i$, whose dynamics are subsequently controlled by positive or negative feedback loops exerted through some of the Ca^{2+}-dependent effector systems and the dynamics of the $[Ca^{2+}]_i$ group of proteins, which, in turn, are supported by homeostasis proteins (Fig. 5 Right). These feedback loops seem to be predominantly mediated by transport of Ca^{2+} ions (through Ca^{2+}-ATPases and Na^+-Ca^{2+} exchangers) and the control of Cav channel activity through changes in membrane potential (electrical signaling), posttranslational modification (including phosphorylation), and signaling through GPCRs. The level of $[Ca^{2+}]_i$ resulting from these activities subsequently regulates a number of Ca^{2+}-dependent effectors (Fig. 5 and Table S2), which may either induce changes in the local architecture and morphology (including cytoskeleton remodeling) or drive second-messenger processes such as changes in the membrane potential (through BK_{Ca} channels), protein phosphorylation and dephosphorylation (through PKC, CaMKII, or PP2B), generation of nitric oxide (through NOS), or release of neurotransmitters. Together, these
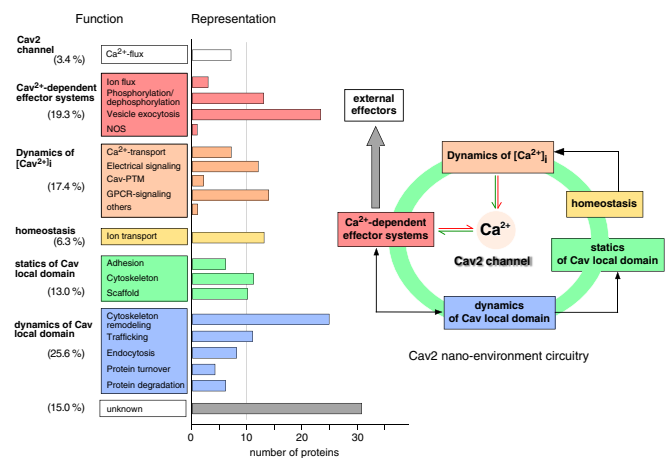
Fig. 5. Representation of cellular functions and operation circuitry of Cav2 nano-environments. (Left) Identified protein constituents of the Cav2 nano-environments grouped into six classes (boxed, numbers denoting relative participation) reflecting their functional significance for the signaling and operation of Cav2 networks. Bars illustrate representation of the respective function in the Cav2 proteome (Table S2). (Right) Operation of Cav2 nano-environments as a functional entity. Arrows in red and green represent positive and negative feedback of or onto free Ca^{2+} ions provided by the Cav2 channels, respectively; arrows in black denote modulatory activity between proteins of the respective functional groups. Details on organization and circuitry are discussed in the main text.
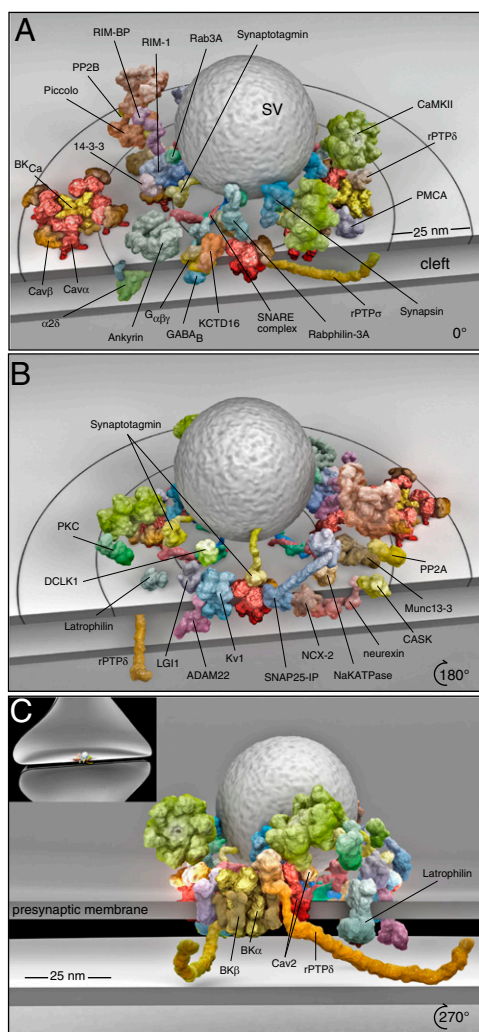
Fig. 6. Molecular modeling of Cav2 nano-environments in the presynapse. Selected proteins of the Cav2 channel proteome with documented localization to the presynaptic compartment arranged to reflect their function (as obtained from public databases), molecular structure (pdb database) (Table S3), abundance (Table 1), and clustering (Fig. 4C). All proteins are represented as space-filling models, and the BK$_{Ca}$-Cav2 complex (A, left side; ~1.6 MDa) (17) may serve as size reference. SV, releasable synaptic vesicle. Views in A–C are related to each other by the indicated rotations around an axis perpendicular to the membrane; (C) is additionally rotated by ~60° around a horizontal axis. (Inset) Projection of the nano-environment into a small synapse (diameter = 1 μm).

effector processes may be regarded as the output of the network that carries the locally integrated Ca^{2+} signal beyond the boundaries of the nano-environments (Fig. 5 Right, external effectors).

Discussion

There is emerging evidence that understanding signal transduction by ion channels (and most likely, other membrane proteins) requires comprehensive analysis of their molecular environment beyond the interaction of pore-forming and auxiliary subunits. So far, however, experimental procedures enabling unbiased and comprehensive access to the environment of membrane proteins have been missing or have just begun to evolve (17–23, 34).

The proteomic approach developed here for identification of the nano-environments of Cav2 channels relied on three key elements: (*i*) appropriate solubilization of protein networks from brain membranes, (*ii*) stringently controlled multiepitope APs together with high-resolution quantitative MS, and (*iii*)

a three-tiered analysis filter to extract the constituents of Cav2 networks. At each step, the approach maintains comprehensiveness while minimizing false-positive protein candidates.

Solubilization of Cav2 channels is intrinsically difficult (33), likely because of their integration into extended protein networks, requiring thorough optimization with quantitative assessment of efficiency (Fig. 1). Digitonin, although an effective solvent of Cav1 channels in skeletal muscle, apparently selected for readily soluble subpopulations of Cav2 channels not integrated into protein networks, as indicated by the low yield of affinity-purified Cav2 protein (Fig. 1B) and the appreciable amount of copurified α2δ reportedly interacting with Cav2 channels primarily during ER-Golgi trafficking (15, 45). In contrast, CL-91 specifically copurified at least 200 different proteins, which, according to database annotations, originated from assembly with Cav2 channels in both plasma membrane and membrane vesicles (Fig. 3 and Table 1). This complexity is specific for Cav2 channels, because rather limited sets of partner proteins were obtained under the same conditions for other ion channels (17, 22, 23). CL-114, a buffer with increased stringency, seemingly interfered with the integrity of protein networks, stripping away the less tightly integrated components.

All APs were performed under conditions of minimized dissociation (of nano-environments); that is, APs used incubation times of ≤2 h at 4 °C and physiological ionic strength. These conditions favor copurification of stably interacting proteins while disfavoring more dynamic protein–protein interactions. Nevertheless, the latter may well be detected by our approach, unless the amount of the remaining fraction(s) drops below a total of ~0.5% of the amount of Cav2 α1.

Target specificity and comprehensiveness are the most critical issues in AP analyses of protein networks. For the Cav2 nano-environments, these issues were effectively addressed by the use of multiple ABs with distinct (and orthogonal) epitopes and a three-tiered filtering, combining thresholds for protein abundance, target specificity, and consistency among different APs (Fig. 1A). In addition, APs from target knockout membranes proved to be very effective negative controls, eliminating more than 70% of all copurified proteins as target-independent background (Fig. 1C). Filtering for consistency further eliminated biases introduced by individual ABs and promoted annotation of proteins robustly copurified with the individual Cav2 channel subtypes (207 of 1,317 relevant proteins) (Fig. 1D). The validity of this procedure is emphasized by the absence of common background proteins, such as nuclear, mitochondrial, or other abundant housekeeping proteins, without introduction of any obvious bias to certain types and classes of proteins (Figs. 3 and 4 and Table 1). In addition, our approach confirmed the majority of proteins reliably identified as direct interactors of Cav2 channels (Table S4, upper half). It should be noted, however, that our filtering operated on the cost of completeness, which means that it likely discarded a portion of true-positive members of Cav2 networks. Thus, proteins with higher interaction dynamics (e.g., Ca^{2+}-dependent interactions), promiscuous binding properties (e.g., proteins interacting with cytoskeletal scaffolds) (46), low expression levels, and/or strong Cav2 subtype preference may have been eliminated. For example, the prototypic Ca^{2+}-binding protein calmodulin, although detected in individual APs, failed the consistency criterion, strongly suggesting that it interacts with Cav2 channels on a more dynamic basis as recently suggested (47) or alternatively, binds to background proteins equivalently well as to Cav2 channels. In addition, lower affinity interactions that may indeed be physiologically used by Cav2 channels might be missed with our approach.

Nevertheless, the Cav2 proteome presented in this study is a comprehensive and unprejudiced analysis of the molecular environments of the P/Q-type, N-type, and R-type Cav channels in the mammalian CNS and extends far beyond previous studies. Of the 200 identified proteins, less than 10% have been biochemically linked to Cav2 channels (Table S4). Moreover, the present proteome provides information on protein isoforms, abundance of

Table 1. Protein constituents of Cav2 channel nano-environments in the brain

Acc. No.	Protein ID	rel. Abundance	Subtype Preference
P54282	Cav2.1	=	N.A.
Q02294	Cav2.2	=	N.A.
Q07652	Cav2.3	=	N.A.
P54283	Cav beta-1	=	A B E
Q8VGC3	Cav beta-2	<	A b E
P54287	Cav beta-3	=	A B E
Q8R0S4	Cav beta-4	=	A B E
P35213	14-3-3 beta	<	B e
P62260	14-3-3 epsilon	=	• B e
P68511	14-3-3 eta	<	B
Q5SSL4	ABR	<<	a b
Q9R1V6	ADAM 22	<	a b e
O88444	ADcyclase1	<<	b e
P23348	Anion exchanger 3	<	b
Q9BXX3	ANKRD 30A	<<	a b e
Q02357	Ankyrin-1	<	a b e
P62744	AP2 sigma-1	=	• B e
P59999	ARPC4	<	b
O70228	ATPase IIA	<<	a B
Q8CCN5	BCAS3	<	e
P08413	CaMKII beta	=	a
P15791	CaMKII delta	=	a
P11730	CaMKII gamma	=	A
P13234	CaMKIV	<<	b
Q63092	CaMKV	<	B e
Q5M9G3	Caprin-1	=	• B e
Q62915	CASK	<<	b
Q9WU82	Catenin beta-1	=	a
P20272	CB1	<<	a
Q8CFN2	CDC42	=	b
Q8CGU4	Centaurin gamma-1	<	• B e
P85515	Centractin	<	• b
Q99JD4	CLAP2	<<	a b e
P11442	Clathrin HC-1	<	B
Q5U2P1	CNNM2	<<	b
P45592	Cofilin-1	=	a b e
P08050	Connexin-43	=	a
Q9Z2F5	CTBP1	=	b
Q5SQX6	CYFP2	<<	a b e
Q62696	DLG1/SAP97	<<	a b
P31016	DLG4/SAP90	<	e
O35824	DNJA2	<<	b
P46101	DPP6	<<	b
P47942	DPYL2	=	B
Q6AYH5	Dynactin subunit 2	<	B
P39052	Dynamin-2	<	a e
Q8BW94	Dynein HC-3	<<	b e
Q9D2N4	Dystobrevin alpha	<	• B
Q9JI90	E3 ligase RNF14	<	a b
Q9WTP0	E41L1	<	a b e
O70318	E41L2	<<	• b
Q9WV92	E41L3	<	a E
P24942	EAAT1/ SLC1A3	=	• B e
Q5VTE0	EF1A3	<	• B
Q60902	EPS15R	<	• B
Q9Y4F1	FARP1	<	B e
Q9UKB1	FBW1B	<	b
P54311	G beta-1	<	a b
Q9Z0U4	GABA$_{B1}$	<	B
O88871	GABA$_{B2}$	<	a b
Q9Z272	GIT1	<	a B e
Q63226	GluR delta-2	<	a e
P19491	GluR-B	<	a b e
P11167	GLUT-1/SLC2A1	<	a e
Q8C419	GPR158	<<	a b
Q8K0U4	HSP 12A	<	a B E
Q9WVE9	Intersectin-1	<	a b
Q96AA8	JKIP2	<	a e
Q9ET77	Junctophilin-3	<<	a b
Q6P5U7	K1239	<<	A B
Q62976	KCa1.1/BKca alpha	<	a B
Q63633	KCC2/SLC12A5	<	A E
Q6WVG3	KCTD12	<	B
Q5DTY9	KCTD16	=	• B
Q50H33	KCTD8	<	B
Q9WV63	KIF2A	<	a b
P28028	Kinase B-raf	<<	a
O08875	Kinase DCLK1	<	a B E
O08679	Kinase MARK2	<<	a
Q5RJI5	Kinase SAD-B	<<	b
P62483	Kv beta-2	=	A B E
P10499	Kv1.1	<	a b
P63142	Kv1.2	<	a b e
P25122	Kv3.1	=	a b
Q01956	Kv3.3	<	• b
O88943	Kv7.2/KCNQ2	<	A B E
Q99MZ6	LASP1	<	a B E
O88917	Latrophilin-1	<	b
Q8K4Y5	LGI1	<	a
Q8K406	LGI3	<	A
Q7TMB7	LPPR4	=	• b E
P70587	LRRC7	<	b
P07722	MAG	<<	b
P15205	MAP1B	<	a B
Q5M7W5	MAP4	<<	a b
Q63560	MAP6	=	A B E
Q3B8Q0	MARE2	<	b
P23385	mGluR-1	<<	b
P31421	mGluR-2	<<	b
P31423	mGluR-4	<<	b
P31424	mGluR-5	<<	a B e
Q63327	MOBP	<	A E
Q63345	MOG	<	a e
P97538	M-Ras	<	b
Q62768	Munc13-1	<<	a b •
Q62770	Munc-13-3	<	a b
Q01728	NaCaExchanger-1 (NCX-1)	<<	b
P48768	NaCaExchanger-2 (NCX-2)	<	a b e
P06685	NaKATPase alpha-1	<	a E
P06686	NaKATPase alpha-2	<	E
P07340	NaKATPase beta-1	<	• E
P54900	Nav beta-2	<<	• b
P04775	Nav1.2	<<	• b
P55161	Nck-associated protein 1	<	a e
Q63372	Neurexin-1 alpha	<<	b
Q5FVQ8	NLRX1	=	B e
P29476	NOS1	=	a e
O88588	PACS1	<	a B
Q01062	PDE2A	<	a b e
Q63716	Peroxiredoxin-1	<	• b
P35704	Peroxiredoxin-2	<	a B
P47860	PFKinase-C	=	A B E
P47858	PFKinase-M	=	A B E
P42356	PI4-kinase	<<	a B e
Q9JKS6	Piccolo	<<	a b
P05696	PKC alpha	<	b
P68403	PKC beta	=	A B E
P63319	PKC gamma	=	A E
P11505	PMCaATPase-1	<	b e
P11506	PMCaATPase-2	<	• E
Q64568	PMCaATPase-3	<	a B e
Q64542	PMCaATPase-4	<	a b e
P62024	PP1 and actin regulator 1	<	a
P62142	PP1B	=	b
Q76MZ3	PP2A-PR65	<	B e
P63329	PP2B alpha (calcineurin)	=	B e
P10536	Rab1B	<	b e
P05712	Rab2A	<	e
Q63941	Rab3B	<	a b
P62824	Rab3C	<	A b
P61107	Rab14	<	a b
P35289	Rab15	<	• b
Q5EB77	Rab18	<	b e
Q6AXT5	Rab21	<	b e
O35963	Rab33B	=	• b •
Q8BHD0	Rab39A	<	a b
Q8BPN8	Rabconnectin-3	<	b
P47709	Rabphilin-3A	<	A B E
Q9EPU0	RENT1	<<	a B
Q62703	Reticulocalbin-2	<<	e
Q64548	Reticulon-1	<<	b
Q9JK11	Reticulon-4/Nogo protein	<	b
P61589	RhoA	=	b e
P84096	RhoG	<	A B
Q5FVC2	RhoGEF-2	<<	• B •
Q5XXR3	RhoGEF-6	<<	b
Q8R4H2	RhoGEF-12	<<	a b
Q9JIR4	RIM 1	<	a
Q9JIR1	RIM-BP2	=	A
Q64487	rPTP-delta	<<	• B
Q64605	rPTP-sigma	<	a B E
P62071	R-RAS2	<	b e
Q5FVJ0	RUFY3/Rap2-IPx	<	B e
P28661	Septin-4	<	b
Q9WVC0	Septin-7	<	B
B0BNF1	Septin-8	<	B e
Q9JI66	SLC4A4/NBC-1	<	a
Q80ZA5	SLC4A10	<	a b e
Q62634	SLC17A7/VGluT1	<	a e
O35458	SLC32A1/GVAT	<	a b
P60881	SNAP25	=	a B E
Q9JJ50	SNAP25-IP HRS-2	<	b
P11507	SRCaATPase-2	=	a •
Q02563	SV2A	<	a
P09951	Synapsin-1	<	A E
Q63537	Synapsin-2	=	a B E
P63045	Synaptobrevin-2	=	B e
Q62910	Synaptojanin-1	<<	a b
Q9Z327	Synaptopodin	<	b
P22831	Synaptoporin	=	e
P29101	Synaptotagmin-2	<	a b
Q9R0N7	Synaptotagmin-7	<	a b
Q9QUH6	SynGAP	<	a
B5DF41	Syntaphilin	<	A b
P32851	Syntaxin-1A	<	B
P61265	Syntaxin-1B	=	• E
P61765	Syntaxin BP-1	<	e
Q9WU70	Syntaxin BP-5	<<	b
Q9Z142	TMEM-33	<	E
Q3U0M1	TPPC9	<	• b e
O70277	TRIM3/Ring finger protein 22	<	a B e
Q0KL02	TRIO	<<	a b
Q9HCF6	TRPM3	<<	a b
P68370	Tubulin alpha-1A	>	a B e
P85108	Tubulin beta-2A	>	a B e
Q3KRE8	Tubulin beta-2B	>	b
P62989	Ubiquitin	=	a
P56399	Ubiquitin thioesterase 5	<	a b e
P70398	Ubiquitin thioesterase FAF-X	<	a b e
P50516	V-ATPase A	<	A B
P62815	V-ATPase B	<	b e
Q8VBE3	V-ATPase H	<	b e
Q8CF97	VCIP135	<<	a b e
Q9ERH3	WDR7	<	a b E
Q8CBE3	WDR37	<	a B
P39447	ZO-1	<	b
Q9Z0U1	ZO-2	<	b

Proteins specifically and consistently identified in APs with *anti-Cav* ABs (Fig. 1A) using CL-91 as solubilization buffer listed in alphabetic order; accession numbers (Acc. No.) refer to the UniProtKB/SwissProt database. Proteins in bold were also identified in APs with CL-114. Molar abundance of proteins relative to the average amount of Cav2 α1 used as reference (rel. abundance) was classified as > if more than 3.3-fold reference amount, = when between 0.33-fold and 3.3-fold of reference, < when between 0.033-fold and 0.33-fold of reference, and << when less than 0.033-fold reference amount. Association of proteins with Cav2.1–2.3 (subtype preference) is given in a three-letter code with A, B, and E denoting Cav2.1 (α1A), Cav2.2 (α1B), and Cav2.3 (α1E), respectively; capital and normal letters reflect very high [(AP(WT)/[AP(IgG)]) ≥ 25] and high [(AP(WT)/[AP(IgG)]) ≥ 10] enrichment by the majority of Cav2 subtype-specific antibodies, respectively, and dots reflect specific identification with individual antibodies only

copurification, and preference for assembly with the individual Cav2 subtypes (Fig. 4A and Table 1). Correlation analyses using these quantitative data identified a number of connections and protein clusters within Cav2 networks and provided links to specific subcellular compartments (Fig. 4C and Fig. S5). All of this information has been organized as protein datasheets (Fig. S5, sample sheet) on a publicly available platform (http://www.channel-proteomes.com) that may serve as a roadmap for ultrastructural and functional analyses of Ca^{2+}-dependent processes and Cav2-mediated signaling in the mammalian brain.

To further promote such investigations, we formulated a molecular model of Cav2 channel-associated networks in the presynaptic compartment, the predominant localization of Cav2 channels in CNS neurons (48, 49), using the spatial constraints set forth by functional and proteomic data. We used a subset of 36 proteins from the Cav2 proteome (Fig. 3 and Table 1) with known presynaptic localization together with database annotations on their structure, function, and protein interactions as well as the biochemical information obtained from this study (Table 1) and experimental constraints (micelles used in our APs had dimensions of ≤70 nm) to generate the 3D model depicted in Fig. 6. Because presynaptic P/Q-type and N-type channels supply the Ca^{2+} for Ca^{2+}-dependent synchronous release of

transmitters, a synaptic vesicle was placed immediately on top of four Cav2 channels (estimate from refs. 4, 50, and 51). Because of inherent structural constraints, only a small number of partner proteins are able to directly interact with the core of individual Cav2 channels. Consequently, Cav2 channels will coassemble with distinct sets of partners, and these core assemblies, potentially involving different Cav2 subtypes, may interact biochemically and functionally to form nano-environments. Within these networks, multiple attachment points may exist, such as between Cav2 channels and the synaptic vesicles, thus generating a high degree of redundancy that enables transmitter release even if single-protein constituents are defective or absent (52). The marked number of connections would require coordinated activities of multiple partners to accomplish complex processes and provides a molecular explanation for the reliability and diversity of Cav2-dependent Ca^{2+} signaling processes.

Materials and Methods

The proteomic approach, including preparation of source material, affinity purification, and high-resolution quantitative nano–LC-MS/MS, were done as described in refs. 22, 23, and 34. Specifications and further details, as well as an extended description of the data-evaluation procedure and correlation analysis, are provided in *SI Materials and Methods*.

1. Berridge MJ, Lipp P, Bootman MD (2000) The versatility and universality of calcium signalling. *Nat Rev Mol Cell Biol* 1:11–21.
2. Clapham DE (2007) Calcium signaling. *Cell* 131:1047–1058.
3. Augustine GJ, Santamaria F, Tanaka K (2003) Local calcium signaling in neurons. *Neuron* 40:331–346.
4. Neher E (1998) Vesicle pools and Ca²⁺ microdomains: New tools for understanding their roles in neurotransmitter release. *Neuron* 20:389–399.
5. Fakler B, Adelman JP (2008) Control of K(ca) channels by calcium nano/microdomains. *Neuron* 59:873–881.
6. Bootman MD, Lipp P, Berridge MJ (2001) The organisation and functions of local Ca²⁺ signals. *J Cell Sci* 114:2213–2222.
7. Rizzuto R, Pozzan T (2006) Microdomains of intracellular Ca²⁺: Molecular determinants and functional consequences. *Physiol Rev* 86:369–408.
8. Catterall WA, Few AP (2008) Calcium channel regulation and presynaptic plasticity. *Neuron* 59:882–901.
9. Dolmetsch R (2003) Excitation-transcription coupling: Signaling by ion channels to the nucleus. *Sci STKE* 2003:PE4.
10. Higley MJ, Sabatini BL (2008) Calcium signaling in dendrites and spines: Practical and functional considerations. *Neuron* 59:902–913.
11. Spitzer NC (2006) Electrical activity in early neuronal development. *Nature* 444:707–712.
12. Catterall WA, Perez-Reyes E, Snutch TP, Striessnig J (2005) International Union of Pharmacology. XLVIII. Nomenclature and structure-function relationships of voltage-gated calcium channels. *Pharmacol Rev* 57:411–425.
13. Arikkath J, Campbell KP (2003) Auxiliary subunits: Essential components of the voltage-gated calcium channel complex. *Curr Opin Neurobiol* 13:298–307.
14. Catterall WA (2000) Structure and regulation of voltage-gated Ca²⁺ channels. *Annu Rev Cell Dev Biol* 16:521–555.
15. Dolphin AC (2009) Calcium channel diversity: Multiple roles of calcium channel subunits. *Curr Opin Neurobiol* 19:237–244.
16. Gingras AC, Gstaiger M, Raught B, Aebersold R (2007) Analysis of protein complexes using mass spectrometry. *Nat Rev Mol Cell Biol* 8:645–654.
17. Berkefeld H, et al. (2006) BK_ca-Cav channel complexes mediate rapid and localized Ca²⁺-activated K⁺ signaling. *Science* 314:615–620.
18. Bildl W, et al. (2004) Protein kinase CK2 is coassembled with small conductance Ca²⁺-activated K⁺ channels and regulates channel gating. *Neuron* 43:847–858.
19. Liu J, Xia J, Cho KH, Clapham DE, Ren D (2007) CatSperbeta, a novel transmembrane protein in the CatSper channel complex. *J Biol Chem* 282:18945–18952.
20. Nadal MS, et al. (2003) The CD26-related dipeptidyl aminopeptidase-like protein DPPX is a critical component of neuronal A-type K⁺ channels. *Neuron* 37:449–461.
21. Schulte U, et al. (2006) The epilepsy-linked Lgi1 protein assembles into presynaptic Kv1 channels and inhibits inactivation by Kvbeta1. *Neuron* 49:697–706.
22. Schwenk J, et al. (2009) Functional proteomics identify cornichon proteins as auxiliary subunits of AMPA receptors. *Science* 323:1313–1319.
23. Zolles G, et al. (2009) Association with the auxiliary subunit PEX5R/Trip8b controls responsiveness of HCN channels to cAMP and adrenergic stimulation. *Neuron* 62:814–825.
24. Vermeulen M, Hubner NC, Mann M (2008) High confidence determination of specific protein-protein interactions using quantitative mass spectrometry. *Curr Opin Biotechnol* 19:331–337.
25. Khanna R, Li Q, Bewersdorf J, Stanley EF (2007) The presynaptic CaV2.2 channel-transmitter release site core complex. *Eur J Neurosci* 26:547–559.
26. Klemmer P, Smit AB, Li KW (2009) Proteomics analysis of immuno-precipitated synaptic protein complexes. *J Proteomics* 72:82–90.
27. Jun K, et al. (1999) Ablation of P/Q-type Ca²⁺ channel currents, altered synaptic transmission, and progressive ataxia in mice lacking the alpha(1A)-subunit. *Proc Natl Acad Sci USA* 96:15245–15250.
28. Ino M, et al. (2001) Functional disorders of the sympathetic nervous system in mice lacking the alpha 1B subunit (Cav 2.2) of N-type calcium channels. *Proc Natl Acad Sci USA* 98:5323–5328.
29. Pereverzev A, et al. (2002) Disturbances in glucose-tolerance, insulin-release, and stress-induced hyperglycemia upon disruption of the Ca(v)2.3 (alpha 1E) subunit of voltage-gated Ca²⁺ channels. *Mol Endocrinol* 16:884–895.
30. Neef J, et al. (2009) The Ca²⁺ channel subunit beta2 regulates Ca²⁺ channel abundance and function in inner hair cells and is required for hearing. *J Neurosci* 29:10730–10740.
31. Berggren PO, et al. (2004) Removal of Ca²⁺ channel beta3 subunit enhances Ca²⁺ oscillation frequency and insulin exocytosis. *Cell* 119:273–284.
32. Burgess DL, Jones JM, Meisler MH, Noebels JL (1997) Mutation of the Ca²⁺ channel beta subunit gene Cchb4 is associated with ataxia and seizures in the lethargic (lh) mouse. *Cell* 88:385–392.
33. Yamaguchi T, Saisu H, Mitsui H, Abe T (1988) Solubilization of the omega-conotoxin receptor associated with voltage-sensitive calcium channels from bovine brain. *J Biol Chem* 263:9491–9498.
34. Schwenk J, et al. (2010) Native GABA(B) receptors are heteromultimers with a family of auxiliary subunits. *Nature* 465:231–235.
35. Yan J, et al. (2008) Profiling the phospho-status of the BK_ca channel alpha subunit in rat brain reveals unexpected patterns and complexity. *Mol Cell Proteomics* 7:2188–2198.
36. Cox J, Mann M (2008) MaxQuant enables high peptide identification rates, individualized p.p.b.-range mass accuracies and proteome-wide protein quantification. *Nat Biotechnol* 26:1367–1372.
37. Burgess DL, et al. (1999) Beta subunit reshuffling modifies N- and P/Q-type Ca²⁺ channel subunit compositions in lethargic mouse brain. *Mol Cell Neurosci* 13:293–311.
38. Reid CA, Bekkers JM, Clements JD (2003) Presynaptic Ca2+ channels: A functional patchwork. *Trends Neurosci* 26:683–687.
39. Schoch S, Gundelfinger ED (2006) Molecular organization of the presynaptic active zone. *Cell Tissue Res* 326:379–391.
40. Rettig J, et al. (1996) Isoform-specific interaction of the alpha1A subunits of brain Ca²⁺ channels with the presynaptic proteins syntaxin and SNAP-25. *Proc Natl Acad Sci USA* 93:7363–7368.
41. Maximov A, Südhof TC, Bezprozvanny I (1999) Association of neuronal calcium channels with modular adaptor proteins. *J Biol Chem* 274:24453–24456.
42. Brittain JM, et al. (2009) An atypical role for collapsin response mediator protein 2 (CRMP-2) in neurotransmitter release via interaction with presynaptic voltage-gated calcium channels. *J Biol Chem* 284:31375–31390.
43. Jiang X, et al. (2008) Modulation of CaV2.1 channels by Ca²⁺/calmodulin-dependent protein kinase II bound to the C-terminal domain. *Proc Natl Acad Sci USA* 105:341–346.
44. Kiyonaka S, et al. (2007) RIM1 confers sustained activity and neurotransmitter vesicle anchoring to presynaptic Ca²⁺ channels. *Nat Neurosci* 10:691–701.
45. Bauer CS, et al. (2009) The increased trafficking of the calcium channel subunit alpha2delta-1 to presynaptic terminals in neuropathic pain is inhibited by the alpha2delta ligand pregabalin. *J Neurosci* 29:4076–4088.
46. Jones LS, Yazzie B, Middaugh CR (2004) Polyanions and the proteome. *Mol Cell Proteomics* 3:746–769.
47. Liu X, Yang PS, Yang W, Yue DT (2010) Enzyme-inhibitor-like tuning of Ca²⁺ channel connectivity with calmodulin. *Nature* 463:968–972.
48. Westenbroek RE, et al. (1992) Biochemical properties and subcellular distribution of an N-type calcium channel alpha 1 subunit. *Neuron* 9:1099–1115.
49. Westenbroek RE, et al. (1995) Immunochemical identification and subcellular distribution of the alpha 1A subunits of brain calcium channels. *J Neurosci* 15:6403–6418.
50. Bucurenciu I, Bischofberger J, Jonas P (2010) A small number of open Ca²⁺ channels trigger transmitter release at a central GABAergic synapse. *Nat Neurosci* 13:19–21.
51. Quastel DM, Guan YY, Saint DA (1992) The relation between transmitter release and Ca²⁺ entry at the mouse motor nerve terminal: Role of stochastic factors causing heterogeneity. *Neuroscience* 51:657–671.
52. Sudhof TC (2004) The synaptic vesicle cycle. *Annu Rev Neurosci* 27:509–547.